Contents lists available at [ScienceDirect](https://www.sciencedirect.com)

Nano Materials Science

journal homepage: www.keaipublishing.com/cn/journals/nano-materials-science/

Emerging properties of non-crystalline phases of graphene and boron nitride based materials

Aleandro Antidormi^a, Luigi Colombo^b, Stephan Roche^{a,c,*}^a Catalan Institute of Nanoscience and Nanotechnology (ICN2), CSIC and BIST, Campus UAB, Bellaterra, 08193, Barcelona, Spain^b Department of Materials Science and Engineering, The University of Texas at Dallas, Richardson, TX, 75080, United States^c ICREA–Institutió Catalana de Recerca i Estudis Avançats, 08010, Barcelona, Spain

ARTICLE INFO

Keywords:

amorphous graphene
amorphous boron nitride
thermal transport
molecular dynamics
amorphous materials
electrical transport

ABSTRACT

We review recent developments on the synthesis and properties of two-dimensional materials which, although being mainly of an sp^2 bonding character, exhibit highly disordered, non-uniform and structurally random morphologies. The emergence of such class of amorphous materials, including amorphous graphene and boron nitride, have shown superior properties compared to their crystalline counterparts when used as interfacial films. In this paper we discuss their structural, vibrational and electronic properties and present a perspective of their use for electronic applications.

1. Introduction

In recent years, graphene and related materials have been evaluated in the ever-growing fields of energy harvesting, solar energy generation, biosensors, reinforcement materials and heat dissipators to cite a few [1–4]. Today these materials are prepared using a variety of synthesis methods, from mechanical and chemical exfoliation to catalytic vapour deposition (CVD). The resulting structures show a multiplicity of atomic morphologies which range from “ultraclean” nearly perfect crystalline films to strongly disordered reduced graphene oxides, polycrystalline graphene and h-BN thin films with varying grain sizes and grain boundaries densities [5–8]. The latter forms of large-scale CVD graphene and h-BN are the most promising materials for emerging nanoelectronic applications such as photodetectors, electrodes, brain implants, wearable devices for health monitoring, ultra-wide bandwidth and low power optical communications systems, and spintronics [9–13]. But current efforts to achieve large single-crystal graphene and h-BN are suffering from a low growth rate and unsuitable substrate materials making production at the industrial scale extremely challenging [7,14].

Recent efforts have succeeded in growing wafer-scale forms of carbon and boron-nitride based materials with a high degree of non-crystallinity, naming such structures as amorphous graphene [15,16] and amorphous boron-nitride (a-BN) respectively [17,18]. In Ref. [15], amorphous carbon monolayers were grown on germanium substrates using conventional CVD at high temperatures ($> 900\text{K}$), and the deposited material

was found to be an electrical (Anderson) insulator. Growing thin non-crystalline films eliminates the need for substrates of high crystalline quality, thus potentially enabling the deposition of an atomically flat dielectric film with sp^2 bonding character [15]. In early 2020, an important milestone was achieved concerning the synthesis, via laser-assisted chemical vapour deposition of free-standing, centimetre scale, continuous monolayer of amorphous graphene [16]. Amorphous graphene, a-G, as an interfacial coating or seed for atomic layer deposition processes presents many advantages for advancing the integration of 2D materials in electronic devices as well as their use for diffusion barriers in magnetic recording devices. However, the relation between the physical properties such as thermal transport and the degree of structural imperfection remains to be fully established for these “new” materials.

Bulk hexagonal boron nitride (h-BN) is a layered material isostructural to graphite, alternating boron and nitrogen atoms in its atomic structure, is an excellent electrical insulator with a band gap of about 5.9 eV. Hexagonal BN is one of the best dielectric substrates for two-dimensional (2D) material-based electronic devices due to its atomically smooth and charge-free interface, with an in-plane lattice constant that is nearly lattice matched to that of graphene, $\Delta a/a$ of about 1.8%. As such, h-BN has shown to be a superior substrate for preserving graphene properties from the invasive interaction with the substrate or interface between graphene and substrate. Although h-BN has been extensively used to demonstrate nearly theoretical carrier mobilities in graphene, the h-BN used for these experiments has been exfoliated from bulk grown

* Corresponding author. Catalan Institute of Nanoscience and Nanotechnology (ICN2), CSIC and BIST, Campus UAB, Bellaterra, 08193, Barcelona, Spain.

E-mail address: stephan.roche@icn2.cat (S. Roche).

<https://doi.org/10.1016/j.nanoms.2021.03.003>

Received 23 December 2020; Accepted 10 February 2021

Available online 27 March 2021

2589-9651/© 2021 Chongqing University. Publishing services by Elsevier B.V. on behalf of KeAi Communications Co. Ltd. This is an open access article under the CC

BY-NC-ND license (<http://creativecommons.org/licenses/by-nc-nd/4.0/>).

crystals of very small area of hundreds of square microns [19–21]. Significant advances have been made in the area of h-BN thin film and bulk crystal growth; however, none of the reports have shown a material which would be simultaneously of high enough crystalline quality and sufficient size to be compatible with integration on wafers and device flows of technological importance.

There has been some progress on the growth of bulk h-BN [22,23], nearly a centimetre on the side, but these processes still face the difficulty of scaling single crystals to large volumes. Growth of large area h-BN thin films have also been reported on metals, polycrystalline as well as textured metals on sapphire [24–26]. However, the issue of film transfer, layer number control, surface roughness and single crystallinity are still major obstacles that have been difficult to overcome. Recently, atomic layer deposition of boron nitride (ALD-BN) using BCl_3 and NH_3 precursors directly on thermal SiO_2 substrates was achieved at a relatively low temperature of 600 C [27], with dielectric properties comparable with that of SiO_2 , while improving carrier mobility of graphene field effect transistors (G-FETs/ALD-BN/ SiO_2) by a factor of two, most likely as a consequence of the lower surface charge density and inert surface of ALD-BN in comparison to that of G-FETs fabricated on bare SiO_2 . It is possible, therefore, that with further growth process improvements and tuning the quality ALD-BN could be improved.

In this context, the recent growth of amorphous boron-nitride (a-BN) with low dielectric constant has sparked a huge interest in the context of microelectronics [17]. Indeed, some of the key requirements for interconnect isolation materials are that they should possess low relative dielectric constants, serve as diffusion barriers against migration of interconnect metals such as copper to prevent shorting and be thermally, chemically and mechanically stable [28]. Amorphous boron nitride, because of its inherent non-crystalline structure and refractory nature in comparison to Si-based low dielectric constant materials, is expected to have lower metal diffusion and thus acting as a better barrier than the low-k counterpart. This non-crystalline material could, in principle, be used for several applications, i.e. integrated circuits where a stable low dielectric constant barrier material is needed, and as a dielectric, below the active 2D film as well as above below the gate electrode, for the integration of 2D materials to achieve higher carrier mobility. The newly synthesised a-BN as thin as 3 nm was deposited directly onto a silicon substrate using inductively coupled plasma-CVD. The resulting material showed a low dielectric constant of less than 2 [17]. Moreover, diffusion barrier tests for this new material demonstrated that it can prevent metal atom migration from the interconnects into the insulator. Together with a high breakdown voltage, these characteristics make a-BN an attractive

and perhaps ideal material for practical electronic applications [17]. A recent publication by Kim et al. [29] reported on potentially superior properties of graphene as an etch stop in comparison to traditional carbon based etch stops, such as diamond like amorphous carbon. Amorphous BN could also be used as an etch stop due its refractory nature, and expected high etch selectivity. Further, given its high sp^2 character, as will be shown later, it may be possible to use a-BN as an interfacial dielectric to mitigate the deleterious properties of other dielectrics such as SiO_2 to achieve higher mobility in graphene.

Lastly hybrid graphene-hBN heterostructures are worth mentioning since they provide a variety of properties which can be adjusted by adjusting the relative ratio of carbon versus boron-nitride atoms, allowing to tune the electronic transport as well as optical properties [30–32]. In particular, the possibility of tuning the inert electronic property of h-BN via grain boundary engineering, with the experimental observation of local density of states variation near grain boundaries in polycrystalline hBN, has also been shown (see Fig. 1) [33]. The interesting electronic transport tunability of such hybrid structures was theoretically analyzed in Ref. [34]. Of particular interest are the in-plane heterostructures combining graphene and hexagonal boron nitride (h-BN) which have been found to provide a new type of blue emission source [35]. By exciting the interface with a laser, Kim and coworkers [35] observed a photoluminescence peak at 410 nm, absent in adjacent graphene and h-BN areas. The intensity of the blue photoluminescence was further increased by six-fold by increasing the “interface length” per unit area by preparing in-plane heterostructures of graphene quantum dots (GQD) on a h-BN monolayer. These structures therefore offer an opportunity to fabricate new types of optoelectronic devices based on inherent resonant defects at graphene/h-BN grain boundaries [35].

The large variety of structural possibilities of graphene and boron nitride-based materials have recently stimulated an intense theoretical effort aimed at exploring the relation between their morphological/chemical aspects and their physical properties. In this respect, atomistic calculations performed via classical molecular dynamics (MD) and tight-binding hamiltonians represent widely employed and successful computational frameworks: they proved to be able to both elucidate features hardly deducible from experiments and to make predictions of structural, thermal and electronic properties, respectively. In particular, classical MD with the employment of empirical potentials has been usefully exploited to explore the atomistic structure of disordered forms of Carbon and defective BN correlating them with their vibrational and thermal properties [36–49]. Such simulations have been also used to perform thin-film depositions and cooling processes “in silico”, thus

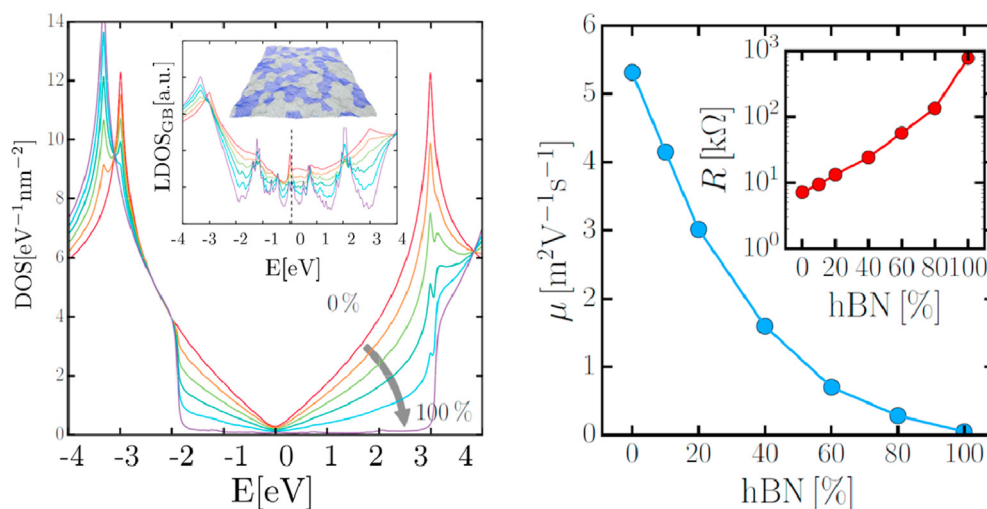


Fig. 1. Left panel: (main frame) evolution of the total density of states of hybrid graphene/hBN structures (% indicates hBN parts); (inset) typical local density of states (LDoS) at grain boundaries between graphene and hBN parts, pinpointing the emergence of impurity states. Right frame: Evolution of the charge mobility (main frame) and sheet resistance (inset) for the same structures. Adapted from Ref. [34].

replicating the experimentally employed protocols on a computer [17, 50–53]. A fundamental feature of classical MD is given by the computational efficiency of the calculations, allowing to study systems made of up to millions of atoms. This factor represents a clear advantage with respect to density-functional-based methods, which are strongly limited to systems of few hundred atoms.

An extremely efficient methodology to describe electronic and transport properties of large-area, spatially complex disordered or nanostructured materials is offered by quasiparticle-based real-space tight-binding (TB) models. Combining this strategy with linear-scaling algorithms also called order-N or O(N) [54], i.e., with computational cost linearly increasing with the number of atoms, the transport properties of a large collection of disordered materials have been investigated, from polycrystalline/defective graphene to hybrid graphene-hBN structures [6,34,55,56].

In this paper, we present the fundamental structural, electronic and thermal properties of amorphous graphene and boron-nitride obtained using molecular dynamics simulations and model Hamiltonians. We show that there exists a large variability of possible structures and degree of disorder which can be obtained by tuning the growth conditions, and that the resulting structures will present tunable electronic and thermal conductivities. These results provide some possible guidelines for further optimizing desired properties of large scale non-crystalline phases of sp^2 -carbon and boron-nitride membranes.

2. Structure, electronic and thermal properties of amorphous graphene

Amorphous graphene has a 2-D structure consisting of 5-6-7 polygons with predominant sp^2 bonding, which can be simulated either using Monte Carlo bond switching algorithm that systematically transforms a crystalline graphene sheet into a disordered structure or through molecular dynamics simulations and quenched from the high temperature liquid state [52]. Kotakoski and coworkers [57] have also used electron irradiation of pristine graphene to create a sp^2 -hybridized one-atom-thick flat carbon membrane with a random arrangement of polygons, including four-membered carbon rings.

The impact of the level of randomness induced by topological disorder on the electronic properties of a-G has already been extensively investigated [56,59]. In contrast to some prior misleading claims, predicting a transition to metallicity when a sufficient amount of disorder is induced in graphene [60], scaling transport studies, using efficient linear scaling approaches [54], have confirmed that, despite the increase of the density of states at low energy compared to pristine graphene, disorder will induce a short mean free path and a charge mobility $\mu \sim 1 - 10 \text{ cm}^2 \text{ V}^{-1} \text{ s}^{-1}$, much lower than clean graphene materials, and inappropriate for most electronic applications [56, 59]. With a localization length of the order of 10 nm, revealed by variable range hopping in low temperature measurements [15], a-G stands as a prototype of Anderson insulating membranes.

The impact of disorder on the electronic properties of a-G is better elucidated by considering samples with a varying degree of non-crystallinity. To this aim, a useful measure of the amount of disorder is expressed by the averaged triatic order parameter \bar{q}_3 , which captures the sp^2 character of a system (see Ref. [58] for its definition), where small values ($\bar{q}_3 < 1$) represent disordered samples and $\bar{q}_3 = 1$ denotes crystalline graphene. Following [58], we will hereafter show the main quantities of interest as a function of such disorder parameter.

The density of states (DOS) of five a-G systems with increasing disorder (decreasing \bar{q}_3) is shown in Fig. 2 (a). The graphene DOS is observed in all cases, accompanied by a broadening of the van-Hove singularities as an effect of disorder. As a result, a strong accumulation of states at the charge neutrality point emerges in the more disordered samples together with an electron-hole asymmetry of the band structure. As recognized in Refs. [55,56], such a feature is due to the presence of odd-membered rings, which are responsible for the creation of quasi-bound states at resonant energies.

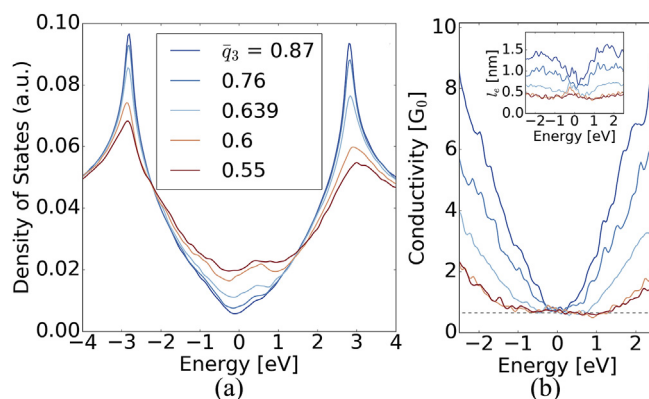


Fig. 2. (a) Total density of states of amorphous graphene samples with different degrees of disorder (different values of triatic order); (b) Semiclassical conductivity of the corresponding samples; (inset) Elastic mean free path vs. energy.

The corresponding conductivity estimated via a Green-Kubo real-space order-N quantum wave packet evolution approach is shown in Fig. 2(b). In the proximity of the charge neutrality point, the conductivity of all the systems converges to the minimum value $\sigma_{min} = 4e^2/\pi h$, which corresponds to the theoretical limit in the diffusive regime [55]. In an energy window of few eV around the charge neutrality point, σ generally increases albeit to a weaker extent in the most disordered systems. For sufficiently disordered samples the conductivity remains almost equal to its minimum semiclassical value σ_{min} in a wide energy range around the Fermi energy, indicating stronger localization effects.

The estimated mean free path (l_e) as a function of energy is derived from the diffusion coefficient calculations and is shown in the inset of Fig. 2(b). A reduction of l_e is observed when increasing disorder in the energy range considered. Specifically, for large values of \bar{q}_3 , the mean free path averaged over the energy range shown decreases linearly with the triatic order ($l_e \propto \bar{q}_3$). For $\bar{q}_3 < 0.6$ the mean free path finally saturates to a value of ~ 0.5 nm, corresponding to about 3 nearest-neighbour distances, in agreement with the theoretical predictions of [56].

A lot of attention has been recently paid to the evolution of thermal properties of aG upon varying the degree of disorder of the structure. Prior theoretical studies employed classical molecular dynamics (MD) and found a significant reduction of the thermal conductivity with increasing disorder [41] while others have explored localization effects of the vibrational modes induced by disorder for a limited number of disorder configurations [43]. In a more recent work [58], a systematic investigation of amorphous graphene based on classical MD has been performed, yielding a self-contained discussion of its structural, vibrational and thermal properties as a function of the degree of disorder. A consistent view of the implications of non-crystallinity on the morphology of the material and on the peculiar vibrational modes that are responsible for heat transport in amorphous graphene has consequently emerged.

Analyzing several atomistic samples of amorphous graphene with different amounts of disorder, the authors of [58] have shown how the presence of topological defects in graphene breaks the regularity of the plane determining a gradual loss of its short- and long-range orders.

The radial distribution functions $g(r)$ (RDFs) of the amorphous graphene samples (Fig. 3(a)) reveal peaks (corresponding to various interatomic distances) broadening when increasing disorder and eventually disappearing for distances larger than a few nearest-neighbour distances. Such a modification in the spatial order of amorphous graphene is associated with an increasing number of non-hexagonal carbon rings and a consequently wider distribution of both the C–C bond lengths and angles (Fig. 3(d)); their mean values are centered at 1.42 \AA and 120° , respectively, with a broadening increasing with disorder. These features have also been experimentally probed in real samples of amorphous graphene [16,61].

A remarkable modification in the structure of amorphous graphene induced by disorder is observed in terms of deviation from planarity.

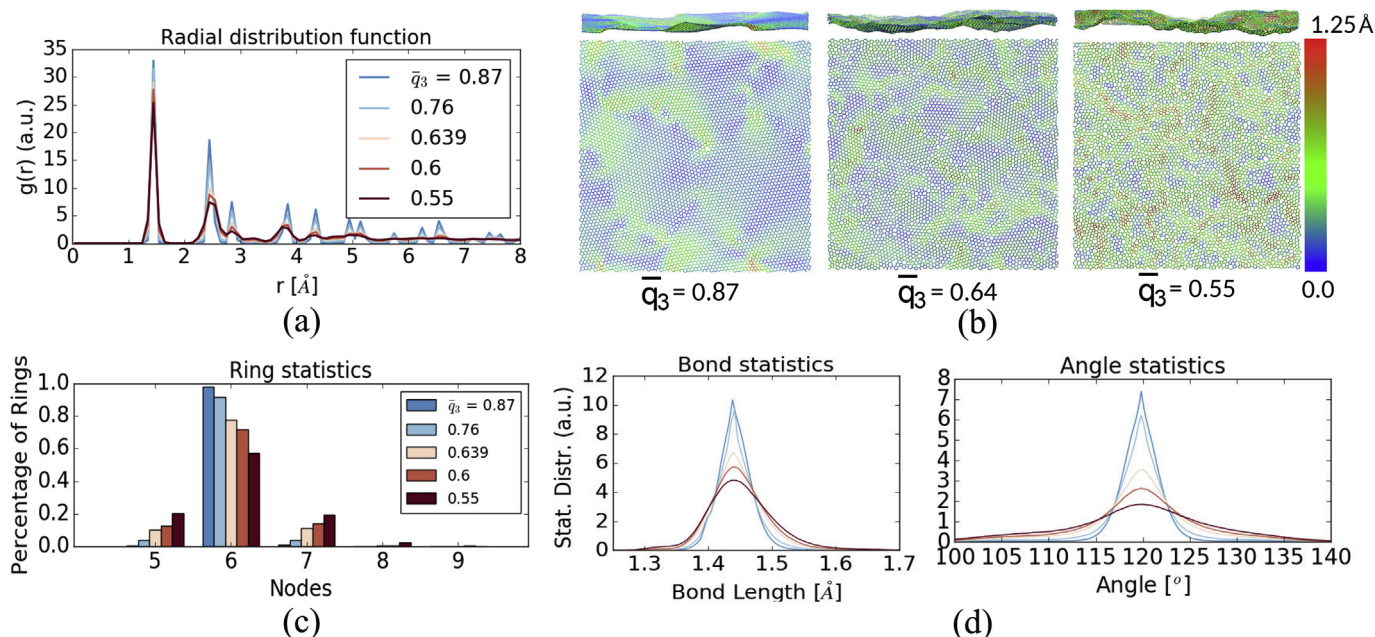


Fig. 3. (a) Radial Distribution functions of amorphous graphene systems for different degrees of disorder (small \bar{q}_3 values denote more amorphous samples); (b) Structural models of three samples with the color map showing the out-of-plane component of the C–C bonds; (c) Ring statistical distribution as a function of \bar{q}_3 ; (d) Statistical distribution of the C–C bond lengths and bond angles. Adapted from Ref. [58].

Non-hexagonal rings are spatial loci where wrinkles are localized in the structure. This can be appreciated by looking at the Fig. 3(b) where the out-of-plane component of the C–C bonds is depicted for three a-G samples. This feature has been also verified both theoretically in Refs. [62,63] and experimentally. Specifically, the authors of [16] extracted a value of interlayer spacing in multilayer amorphous graphene of

approximately 0.6 nm; this value is almost twice as large of that of graphene, in agreement with the disorder-induced roughness predicted theoretically. As also discussed in Ref. [58] and shown in Fig. 3(b), the resulting roughness of amorphous graphene is strongly related to the disorder of the material, with more disordered samples having a stronger deviation from planarity.

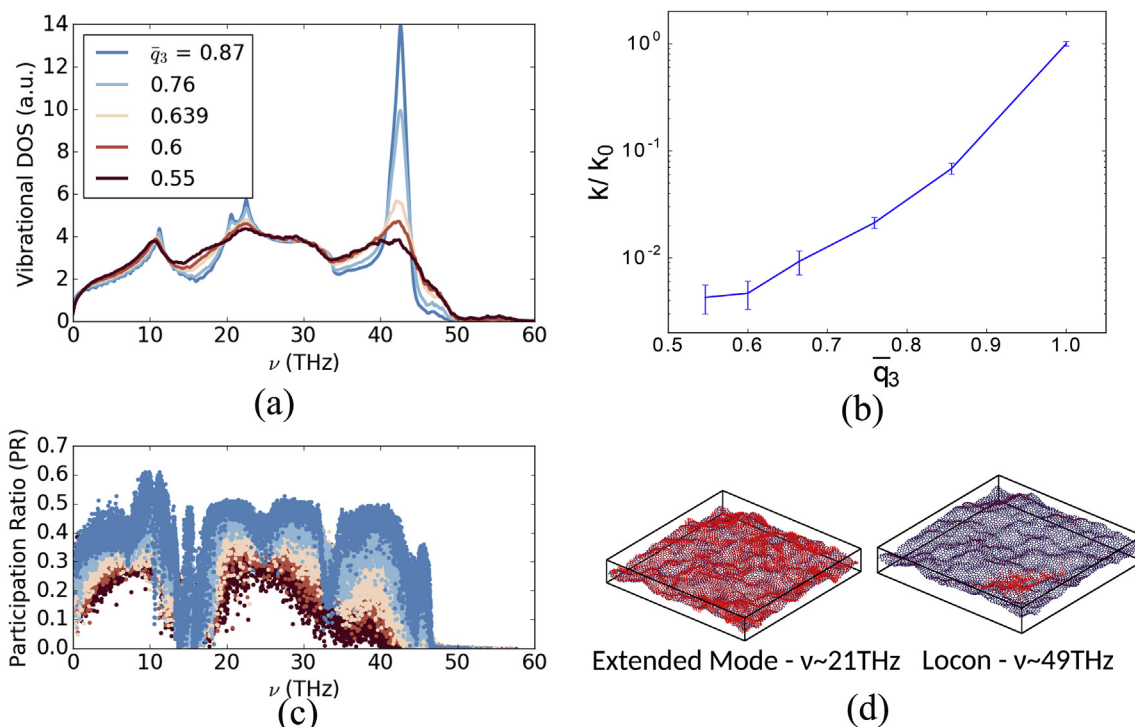


Fig. 4. (a) Vibrational density of states (VDOS) of amorphous graphene systems for different degrees of disorder; (b) Participation Ratio (PR) of the vibrons in the various samples as a function of frequency. (c) Thermal conductivity of the a-G systems at $T = 300\text{K}$ vs. \bar{q}_3 normalized wrt to the corresponding value of crystalline system κ_0 ; (d) Atomic displacements for two vibrons in the sample with $\bar{q}_3 = 0.55$: a diffusion on the left and a locon on the right. The (properly scaled) displacements are depicted as red vectors superimposed on blue dots representing atoms. Adapted from Ref. [58].

The specific structural features of amorphous graphene are clearly expected to play a major role in the determination of the vibrational properties of the material, eventually affecting the thermal conductivity. In this respect, it has been shown [16,58] that the presence of disorder in a-G is ultimately responsible for a substantial change in both the spatial character of the vibrations and their effect on thermal transport.

The consequences of non-crystallinity on the vibrational properties of the material can be observed from the vibrational density of states (VDOS) shown in Fig. 4(a) as a function of the triatic order parameter. While the VDOS of the more crystalline systems present peaks reminiscent of the phonon bands of crystalline graphene, the band separation is lost when increasing disorder and no bands can be identified in the most disordered sample.

More remarkably, the amount of disorder in amorphous graphene determines a substantial modification of the spatial extension of the vibrational modes, inducing a strong localization of the modes. The participation ratio (PR) of the vibrons in the various systems as a function of frequency is shown in Fig. 4(b) ($PR \sim 1$ for extended modes and $PR \sim 0$ for localized ones, respectively). The atomic displacement field of an extended mode and of a locon is shown in Fig. 4(d) for the same sample. Vibrational modes in amorphous samples are more spatially localized, involving a smaller number of atoms sizeably vibrating around their equilibrium position. Furthermore, such a localization effect is dependent on the amount of disorder and is observed across the frequency spectrum.

A more extensive numerical analysis of the vibrational modes in amorphous graphene reveals that the spatial localization of the vibrons in the material is also accompanied by a disorder-induced change of the fundamental mechanism of heat transport of the single modes [43,58]. When disorder is present in the system, extended vibrons called *diffusons* appear in the higher frequency range of the spectrum: they are characterized by a random field of atomic displacements and dynamically contribute to heat transfer by scattering diffusively along the sample. They differ from *propagons*, which are mainly found at low frequency and are able to propagate without scattering across the material for more than a few interatomic distances. The frequency range dominated by diffusons increases with disorder, with a consequently lower value of the so-called *Ioffe-Regel limit* [64].

Both the localization of the modes and the emergence of diffusive modes along with propagons contribute to our understanding of the reduction of the thermal conductivity experimentally observed in amorphous graphene. In this respect, modal analysis based on the Green-Kubo formalism [65] has proved that a) the most effective modes in carrying heat in such structures are the low-frequency propagons and b) the localized modes are less effective for heat transport with respect to extended modes. These findings offer a clear explanation of the strong reduction of thermal conductivity in amorphous graphene with respect to crystalline graphene: the κ of amorphous graphene decreases with disorder by up to more than two orders of magnitude (Fig. 4(c)).

3. Structure, electronic and thermal properties of amorphous BN

Amorphous Boron Nitride (a-BN) has been recently shown to be very promising as a low dielectric constant material, with a dielectric constant smaller than 2 [17]. Among all, future electronics could largely benefit from the use of a-BN, opening the way to efficient low dielectric constant barrier materials that could benefit current device technology scaling as well as the integration of two-dimensional materials. In this respect, the comparatively high density of the material ($\sim 2.1 \text{ g/cm}^3$) also plays a fundamental role, making it an effective barrier against metal diffusion, which is also a key requirement for next-generation insulating materials. The exceptional properties of a-BN clearly depend on its intrinsically disordered nature. Consequently, the formidable task of understanding

the relationship between its morphological/chemical properties and the resulting electrical/thermal performance is urgently needed.

The unveiling of the fundamental features of a-BN through atomistic simulations has already greatly helped elucidate the main properties of its structural features. In particular, simulation of the chemical vapour deposition process has allowed the authors of [17] to explore the disordered nature of a-BN films. Fig. 5(a) shows an image taken during the deposition of Boron and Nitrogen atoms on a Si substrate simulated via classical molecular dynamics. The simulation was used to grow a 3 nm thick BN film under similar conditions as for experimentally fabricated samples. For the simulation details we refer the reader to the Methods' section. It is clear by visual inspection of Fig. 5(a) that both short- and long-range order is absent in the deposited BN film. The radial distribution functions shown in Fig. 5(b) numerically confirm this evidence: no peak can be identified for distances larger than 4 Å. In addition, the first peak, found at a distance of about 1.43 Å, is mostly due to the B–N bond length, ruling out the possibility of homopolar bonds in the material.

The corresponding statistical distribution of the bond angles in Fig. 5(c) shows an average value at about 120°, also pointing to a locally well-defined chemical environment for both boron and nitrogen atoms. Remarkably, among all of the atoms in the sample, more than 58% are sp^2 -hybridized, i.e. have coordination number equal to 3, whereas 40% present coordination number 4, all of the remaining atoms being undercoordinated. A visual insight of this finding can be gained from Fig. 5(d) where a section of the a-BN sample is shown with atoms depicted in different colors depending on their coordination number n_c : in red we show atoms with coordination number 3, in cyan those with $n_c = 4$, yellow $n_c = 2$ and blue $n_c = 1$. It is also important to acknowledge that the chemical bonding state of a-BN, i.e. sp^2/sp^3 has been already observed experimentally via XPS [17].

Concerning the electronic properties, the disruption of the structural ordering in a-BN affects the electronic properties by slightly reducing the energy bandgap by ~ 0.2 eV due to defect-induced gap states (see Fig. 6). Those states, even if forming an impurity band close to the bulk band edges, are however not conducting and a-BN remains a strong insulator.

The thermal properties of a-BN are also governed by the topologically disordered morphology, leading to a comparatively small value of thermal conductivity. Fig. 7 shows the value of in-plane κ of a-BN films with different thickness. A bulk value of $\kappa \sim 4.0 \text{ W/(mK)}^{-1}$ is obtained for thicknesses larger than 1 nm. Such distance is consequently larger than the phonon mean free path of the material. A slightly smaller value of the thermal conductivity is found for thinner films, reaching the minimum for an a-BN monolayer: in this case, a value of κ two orders of magnitude smaller than the conductivity of a monolayer of h-BN is observed.

4. Summary and conclusions

The structural, vibrational, and electronic properties of amorphous graphene and boron nitride were presented. This new class of materials exhibits a highly disordered structural state with some properties superior to their crystalline counterparts when used as interfacial materials. In particular, the bonding state of a-BN was found to be predominantly of an sp^2 character by molecular dynamics and supported by recent experimental data. The data presented and reviewed in this paper is of great significance for both the 2D materials community as well as the electronics industry. Because of the difficulty in growing large area single crystal h-BN, a-BN with its predominantly sp^2 bonding character could be particularly useful as an interfacial dielectric to screen impurity and defect charges from traditional dielectric substrates. Amorphous graphene on the other hand could be a good diffusion barrier without grain boundaries for many electronic applications especially as the electronics industry scales transistors to the sub 5 nm range.

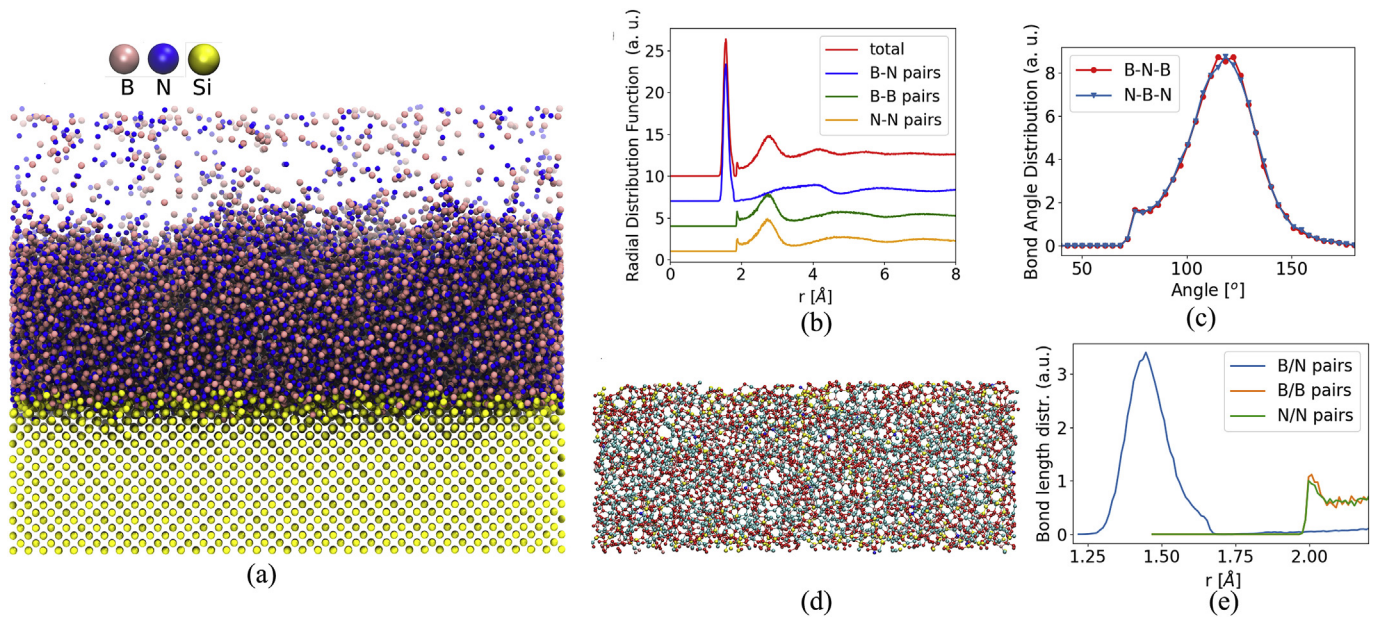


Fig. 5. (a) Image of a film of a-BN deposited on a Silicon substrate extracted from a computer-simulated process; (b) Radial distribution functions (total and chemically resolved) of a-BN: functions are rigidly shifted for the sake of clarity; (c) Statistical distribution of the chemically-resolved bond angles; (d) Section of the a-BN atomistic sample from (a) with 5 thickness; atoms are shown with different colors depending on their coordination number (cyan, 4; red, 3; yellow, 2; blue, 1); e) Statistical distribution of the chemically-resolved bond lengths.

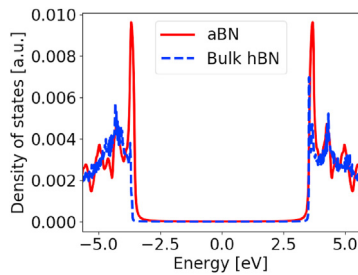


Fig. 6. Total density of states computed via tight-binding approach of a-BN and bulk h-BN systems with 5000 atoms. The tight-binding parameters used in the calculation are presented in Ref. [66].

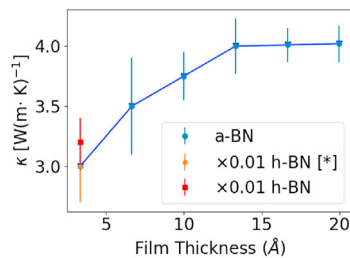


Fig. 7. In-plane thermal conductivity of a-BN films as a function of the film thickness at $T = 300\text{K}$. Values for monolayer hBN are also shown. [*] data are taken from Ref. [34].

5. Methods

5.1. Amorphous graphene

In order to build atomistic samples of amorphous graphene with different degree of disorder, we employed a simulated quench-from-melt method, consisting in cooling a crystalline system from its melt state with different cooling rates. Cooling rates in the range [50K/ps, 1000K/ps] have been employed in this work. As it is shown in Ref. [58], slower

cooling rates determine more crystalline samples (larger \bar{q}_3). The final systems considered in this work use a number of atoms as large as 10032 atoms, with a linear dimension of ~ 160 . Classical molecular dynamics has been adopted to carry out all the calculations, as implemented in the open source LAMMPS package [67]. To extract the vibrational properties of the resulting systems, we computed and diagonalized the dynamical matrix. From the knowledge of the eigenvectors e_s and eigenvalues ω_s^2 with $s = 1, \dots, 3N$ where N is the number of atoms in the sample, the vibrational density of states and the participation ratio (PR) are eventually computed. The PR is given by

$$PR_s \equiv \frac{1}{N} \frac{\left(\sum_{i=1}^N e_{i,s}^2\right)^2}{\sum_{i=1}^N e_{i,s}^4} \quad (1)$$

with $e_{i,s}$ being the i -th component of the s -th eigenmode. Equilibrium molecular dynamics runs have been employed for the calculation of thermal conductivity at $T = 300\text{K}$ via the Green-Kubo formula. Heat flux correlations have been extracted from evolutions of the systems as long as 10ns with a timestep of 0.25 fs. The final value of thermal conductivity of each sample has been averaged over six independent trajectories. The details on the computational protocol used, the study of the reliability of the force-field and a comparison of the simulated samples with experiments can be found in Ref. [58].

The electronic and transport properties of amorphous graphene have been studied with a $\pi - \pi^*$ orthogonal tight-binding (TB) model with nearest neighbour hopping $\gamma_0 = 2.8 \text{ eV}$ [56] and zero onsite energies. No modification of these parameters has been introduced as a function of the interatomic distances, since the topological disorder is the main factor affecting the electronic properties of such systems. The corresponding quantum transport features have been analyzed using a real-space order- N quantum wave packet evolution approach allowing to derive the Kubo-Greenwood conductivity [54]. In this theoretical framework the formula of electron conductivity as a function of energy E reads $\sigma(E) = e^2 \rho(E) \tilde{D}(E)$ where $\rho(E) = \text{Tr} \delta(E - \hat{H})$ is the total density of states, \hat{H} the tight-binding hamiltonian whereas $\tilde{D}(E)$ is the long-time limit of the diffusion coefficient $D(E, t) = \frac{\partial}{\partial t} \Delta X^2(E, t)$. By following the evolution of a wave packet in the sample, the mean squared displacement $\Delta X^2(E, t)$

can be computed using an efficient decomposition in terms of Chebyshev polynomials [54]. In this work the conductivity has been averaged over 100 different randomly chosen wavepackets employing a decomposition with 5000 polynomials. The elastic mean free path is finally derived from the maximum of the diffusion coefficient $D_{max}(E, t)$ as $l_e(E) = 2D_{max}(E, t)/v(E)$ where $v(E)$ is the carrier velocity.

5.2. Amorphous Boron Nitride

The generation of the 3D a-BN film has been performed replicating “in silico” the process of deposition of Boron and Nitrogen atoms on a Silicon substrate held at constant temperature ($T = 673K$) and constant volume using a Nosé-Hoover thermostat. Boron and Nitrogen atoms are allowed to settle and thermalize at the substrate temperature. The final system consists of more than 40000 atoms and the details of the computation protocol employed are given in Ref. [17]. The thermal conductivity values of a-BN films shown in Fig. 7 have been computed via standard equilibrium molecular dynamics methods, using the same interatomic potential of [17] and protocol parameters of [58]. Specifically, six independent runs as long as 10 ns in the NVT ensemble have been employed to statistically average the heat-flux autocorrelations. The density of states and the electrical conductivity of aBN samples have been computed using the tight-binding parameters from Ref. [66] with 50 wavepackets and 5000 Chebyshev polynomials.

The authors thank Hyeon-Suk Shin, Manish Chhowalla and Hyeon-Jin shin for fruitful discussion. AA and SR are supported by Modelling Charge and Heat transport in 2D-materials based Composites - MECHANIC reference number: PCI2018-093120 funded by Ministerio de Ciencia, Innovación y Universidades and the European Union Horizon 2020 research and innovation programme under Grant Agreement No. 881603 (Graphene Flagship). ICN2 is funded by the CERCA Programme/Generalitat de Catalunya, and is supported by the Severo Ochoa program from Spanish MINECO (Grant No. SEV-2017-0706).

Declaration of competing interest

The authors declare no competing financial interests.

References

- [1] A.C. Ferrari, F. Bonaccorso, V. Fal'ko, K.S. Novoselov, S. Roche, P. Bøggild, S. Borini, F.H.L. Koppens, V. Palermo, N. Pugno, J.A. Garrido, R. Sordan, A. Bianco, L. Ballerini, M. Prato, E. Lidorikis, J. Kivioja, C. Marinelli, T. Ryhänen, A. Morpurgo, J.N. Coleman, V. Nicolosi, L. Colombo, A. Fert, M. Garcia-Hernandez, A. Bachtold, G.F. Schneider, F. Guinea, C. Dekker, M. Barbone, Z. Sun, C. Galiotis, A.N. Grigorenko, G. Konstantatos, A. Kis, M. Katsnelson, L. Vandersypen, A. Loiseau, V. Morandi, D. Neumaier, E. Treossi, V. Pellegrini, M. Polini, A. Tredicucci, G.M. Williams, B. Hee Hong, J.-H. Ahn, J. Min Kim, H. Zirath, B.J. van Wees, H. van der Zant, L. Occhipinti, A. Di Matteo, I.A. Kinloch, T. Seyller, E. Quesnel, X. Feng, K. Teo, N. Rupesinghe, P. Hakonen, S.R.T. Neil, Q. Tannock, T. Löfwander, J. Kinaret, *Nanoscale* 7 (2015) 4598.
- [2] Santosh Tiwari K., Sumanta Sahoo, Nannan Wang, Andrzej Huczko, Graphene research and their outputs: Status and prospect, *Journal of Science: Advanced Materials and Devices* 5 (2020) 10–29, <https://doi.org/10.1016/j.jsamd.2020.01.006>.
- [3] C. Backes, A.M. Abdelkader, C. Alonso, A. Andrieux-Ledier, R. Arenal, J. Azpeitia, N. Balakrishnan, L. Banszerus, J. Barjon, R. Bartali, S. Bellani, C. Berger, R. Berger, M.M.B. Ortega, C. Bernard, P.H. Beton, A. Beyer, A. Bianco, P. Bøggild, F. Bonaccorso, G.B. Barin, C. Botas, R.A. Bueno, D. Carriazo, A. Castellanos-Gomez, M. Christian, A. Ciesielski, T. Ciuk, M.T. Cole, J. Coleman, C. Coletti, L. Crema, H. Cun, D. Dasler, D.D. Fazio, N. Díez, S. Drieschner, G.S. Dueschner, R. Fasel, X. Feng, A. Fina, S. Forti, C. Galiotis, G. Garberoglio, J.M. García, J.A. Garrido, M. Gibertini, A. Götzhäuser, J. Gómez, T. Greber, F. Hauke, A. Hemmi, I. Hernandez-Rodriguez, A. Hirsch, S.A. Hodge, Y. Huttel, P.U. Jepsen, I. Jimenez, U. Kaiser, T. Kaplas, H. Kim, A. Kis, K. Papagelis, K. Kostarelos, A. Krajewska, K. Lee, C. Li, H. Lipsanen, A. Liscio, M.R. Lohe, A. Loiseau, L. Lombardi, M.F. López, O. Martin, C. Martín, L. Martínez, J.A. Martín-Gago, J.J. Martínez, N. Marzari, Á. Mayoral, J. McManus, M. Melucci, J. Méndez, C. Merino, P. Merino, A.P. Meyer, E. Miniussi, V. Miseikis, N. Mishra, V. Morandi, C. Munuera, R. Muñoz, H. Nolan, L. Ortolani, A.K. Ott, I. Palacio, V. Palermo, J. Parthenios, I. Pasternak, A. Patane, M. Prato, H. Prevost, V. Prudkovskiy, N. Pugno, T. Rojo, A. Rossi, P. Ruffieux, P. Samorì, L. Schué, E. Setijadi, T. Seyller, G. Speranza, C. Stampfer, I. Stenger, W. Strupinski, Y. Svirko, S. Taioli, K.B.K. Teo, M. Testi, F. Tomarchio, M. Tortello, E. Treossi, A. Turchanin, E. Vazquez, E. Villaro, P.R. Whelan, Z. Xia, R. Yakimova,

- S. Yang, G.R. Yazdi, C. Yim, D. Yoon, X. Zhang, X. Zhuang, L. Colombo, A.C. Ferrari, M. Garcia-Hernandez, *2D Mater.* 7 (2020), 022001.
- [4] J. Wang, F. Ma, M. Sun, *RSC Adv.* 7 (2017) 16801.
- [5] R. Tarcan, O. Todor-Boer, I. Petrovai, C. Leordean, S. Astilean, I. Botiz, J. Mater. Chem. C 8 (2020) 1198.
- [6] A.W. Cummings, D.L. Duong, V.L. Nguyen, D. Van Tuan, J. Kotakoski, J.E. Barrios Vargas, Y.H. Lee, S. Roche, *Adv. Mater.* 26 (2014) 5079.
- [7] J. Zhang, L. Sun, K. Jia, X. Liu, T. Cheng, H. Peng, L. Lin, Z. Liu, *ACS Nano* 14 (2020) 10796.
- [8] Y. Bai, J. Zhang, Y. Wang, Z. Cao, L. An, B. Zhang, Y. Yu, J. Zhang, C. Wang, *ACS Applied Nano Materials* 2 (2019) 3187, <https://doi.org/10.1021/acsnm.9b00502>.
- [9] S. Roche, J. Åkerman, B. Beschoten, J.-C. Charlier, M. Chshiev, S.P. Dash, B. Dlubak, A.M. Lara, A. Fert, M. Guimarães, F. Guinea, I. Grigorieva, C. Schönenberger, P. Seneor, C. Stampfer, S.O. Valenzuela, X. Waintal, B. van Wees, *2D Mater.* 2 (2015), 030202.
- [10] M. Romagnoli, V. Soriano, M. Midrio, F.H.L. Koppens, C. Huyghebaert, D. Neumaier, P. Galli, W. Templ, A. D'Errico, A.C. Ferrari, *Nature Reviews Materials* 3 (2018) 392–414.
- [11] D. Akinwande, C. Huyghebaert, C.-H. Wang, M.I. Serna, S. Goossens, L.-J. Li, H.-S.P. Wong, F.H.L. Koppens, *Nature* 573 (2019) 507.
- [12] N. Schaefer, R. Garcia-Cortadella, J. Martínez-Aguilar, G. Schwesig, X. Illa, A.M. Lara, S. Santiago, C. Hébert, G. Guirado, R. Villa, A. Sirota, A. Guimera-Brunet, J.A. Garrido, *2D Mater.* 7 (2020), 025046.
- [13] K. Kanahashi, N. Tanaka, Y. Shoji, M. Maruyama, I. Jeon, K. Kawahara, M. Ishihara, M. Hasegawa, H. Ohta, H. Ago, et al., *npj 2D Materials and Applications* 3 (2019) 1.
- [14] X. Sun, L. Lin, L. Sun, J. Zhang, D. Rui, J. Li, M. Wang, C. Tan, N. Kang, D. Wei, H.Q. Xu, H. Peng, Z. Liu, *Small* 14 (2018) 1702916.
- [15] W.-J. Joo, J.-H. Lee, Y. Jang, S.-G. Kang, Y.-N. Kwon, J. Chung, S. Lee, C. Kim, T.-H. Kim, C.-W. Yang, U.J. Kim, B.L. Choi, D. Whang, S.-W. Hwang, *Science Advances* 3 (2017), <https://doi.org/10.1126/sciadv.1601821>.
- [16] C.-T. Toh, H. Zhang, J. Lin, A.S. Mayorov, Y.-P. Wang, C.M. Orofeo, D.B. Ferry, H. Andersen, N. Kakenov, Z. Guo, I.H. Abidi, H. Sims, K. Suenaga, S.T. Pantelides, B. Özyilmaz, *Nature* 577 (2020) 199.
- [17] S. Hong, C.-S. Lee, M.-H. Lee, Y. Lee, K.Y. Ma, G. Kim, S.I. Yoon, K. Ihm, K.-J. Kim, T.J. Shin, S.W. Kim, E.-c. Jeon, H. Jeon, J.-Y. Kim, H.-I. Lee, Z. Lee, A. Antidormi, S. Roche, M. Chhowalla, H.-J. Shin, H.S. Shin, *Nature* 582 (2020) 511.
- [18] B. Zhong, X. Zhang, L. Xia, Y. Yu, G. Wen, *Mater. Des.* 120 (2017) 266.
- [19] J. Sun, C. Lu, Y. Song, Q. Ji, X. Song, Q. Li, Y. Zhang, L. Zhang, J. Kong, Z. Liu, *Chem. Soc. Rev.* 47 (2018) 4242.
- [20] C.R. Dean, A.F. Young, I. Meric, C. Lee, L. Wang, S. Sorgenfrei, K. Watanabe, T. Taniguchi, P. Kim, K.L. Shepard, J. Hone, *Nat. Nanotechnol.* 5 (2010) 722.
- [21] H. Jeong, D.Y. Kim, J. Kim, S. Moon, N. Han, S.H. Lee, O.F.N. Okello, K. Song, S.-Y. Choi, J.K. Kim, *Sci. Rep.* 9 (2019) 5736.
- [22] S. Liu, R. He, L. Xue, J. Li, B. Liu, J.H. Edgar, *Chem. Mater.* 30 (2018) 6222, <https://doi.org/10.1021/acs.chemmater.8b02589>.
- [23] B. Matsos, W. Hao, Y. Li, V. V. a Ciles, V. Garnier, P. Steyer, B. Toury, C. Marichy, C. Journet, *J. Phys.: Materials* 3 (2020), 034002.
- [24] Y. Uchida, S. Nakandakari, K. Kawahara, S. Yamasaki, M. Mitsuahara, H. Ago, *ACS Nano* 12 (2018) 6236.
- [25] A.B. Taslim, H. Nakajima, Y.-C. Lin, Y. Uchida, K. Kawahara, T. Okazaki, K. Suenaga, H. Hibino, H. Ago, *Nanoscale* 11 (2019) 14668.
- [26] S. Sonde, A. Dolocan, N. Lu, C. Corbet, M.J. Kim, E. Tutuc, S.K. Banerjee, L. Colombo, *2D Mater.* 4 (2017), 025052.
- [27] J. Lee, A.V. Ravichandran, J. Mohan, L. Cheng, A.T. Lucero, H. Zhu, Z. Che, M. Catalano, M.J. Kim, R.M. Wallace, A. Venugopal, W. Choi, L. Colombo, J. Kim, *ACS Appl. Mater. Interfaces* 12 (2020) 36688.
- [28] M. Moore, Institute of Electrical and Electronics Engineers, Piscataway, New Jersey, USA (2017).
- [29] S.W. Kim, M. Seol, Y. Cho, K.W. Shin, D. Lee, S.-J. Jeong, H. Lee, J.G. Chung, H.-M. Kim, K.-B. Kim, S. Park, H.-J. Shin, *ACS Applied Nano Materials* 3 (2020a) 4635.
- [30] M.P. Levendorf, C.-J. Kim, L. Brown, P.Y. Huang, R.W. Havener, D.A. Muller, *J. Park, Nature* 488 (2012) 627.
- [31] Z. Liu, L. Ma, G. Shi, W. Zhou, Y. Gong, S. Lei, X. Yang, J. Zhang, J. Yu, K.P. Hackenberg, A. Babakhani, J.-C. Idrobo, R. Vajtai, J. Lou, P.M. Ajayan, *Nat. Nanotechnol.* 8 (2013) 119.
- [32] C. Zhang, S. Zhao, C. Jin, A.L. Koh, Y. Zhou, W. Xu, Q. Li, Q. Xiong, H. Peng, Z. Liu, *Nat. Commun.* 6 (2015) 6519.
- [33] Q. Li, X. Zou, M. Liu, J. Sun, Y. Gao, Y. Qi, X. Zhou, B.I. Yakobson, Y. Zhang, Z. Liu, *Nano Lett.* 15 (2015) 5804.
- [34] J.E. Barrios-Vargas, B. Mortazavi, A.W. Cummings, R. Martinez-Gordillo, M. Pruneda, L. Colombo, T. Rabczuk, S. Roche, *Nano Lett.* 17 (2017) 1660.
- [35] G. Kim, K.Y. Ma, M. Park, M. Kim, J. Jeon, J. Song, J.E. Barrios-Vargas, Y. Sato, Y.-C. Lin, K. Suenaga, S. Roche, S. Yoo, B.-H. Sohn, S. Jeon, H.S. Shin, *Nat. Commun.* 11 (2020) 5359.
- [36] V. Kapko, D.A. Drabold, M.F. Thorpe, *Phys. Status Solidi B* 247 (2010) 1197.
- [37] E. Holmström, J. Fransson, O. Eriksson, R. Lizárraga, B. Sanyal, S. Bhandary, M.I. Katsnelson, *Phys. Rev. B* 84 (2011) 205414.
- [38] Y. Li, F. Inam, A. Kumar, M. Thorpe, D. Drabold, *Phys. Status Solidi B* 248 (2011) 2082.
- [39] B. Bhattarai, P. Biswas, R. Atta-Fynn, D.A. Drabold, *Phys. Chem. Chem. Phys.* 20 (2018) 19546.
- [40] Z. Fan, L.F.C. Pereira, P. Hirvonen, M.M. Ervasti, K.R. Elder, D. Donadio, T. Ala-Nissila, A. Harju, *Phys. Rev. B* 95 (2017) 144309.
- [41] B. Mortazavi, S. Ahzi, *Carbon* 63 (2013) 460.
- [42] B. Mortazavi, Z. Fan, L.F.C. Pereira, A. Harju, T. Rabczuk, *Carbon* 103 (2016) 318.
- [43] T. Zhu, E. Ertekin, *Nano Lett.* 16 (2016) 4763.

- [44] A. Bagri, S.-P. Kim, R.S. Ruoff, V.B. Shenoy, *Nano Lett.* 11 (2011) 3917, <https://doi.org/10.1021/nl202118d>, PMID: 21863804.
- [45] V.L. Deringer, G. Csányi, *Phys. Rev. B* 95 (2017), 094203.
- [46] B. Mortazavi, L.F.C. Pereira, J.-W. Jiang, T. Rabczuk, *Sci. Rep.* 5 (2015) 1.
- [47] B. Mortazavi, Y. Rémond, *Phys. E Low-dimens. Syst. Nanostruct.* 44 (2012) 1846.
- [48] K.E. Eshkalak, S. Sadeghzadeh, M. Jalaly, *Phys. E Low-dimens. Syst. Nanostruct.* 104 (2018) 71.
- [49] S. Liu, J. Comer, A.C. Van Duin, D.M. Van Duin, B. Liu, J.H. Edgar, *Nanoscale* 11 (2019) 5607.
- [50] R. Ravinder, R. Kumar, M. Agarwal, N.A. Krishnan, *Sci. Rep.* 9 (2019) 1.
- [51] V.V. Hoang, *Phys. B (Amsterdam, Neth.)* 456 (2015) 50.
- [52] A. Kumar, M. Wilson, M.F. Thorpe, *J. Phys. Condens. Matter* 24 (2012) 485003.
- [53] A. Antidormi, S. Roche, L. Colombo, *J. Phys. Math.* 3 (2019), 015011.
- [54] Z. Fan, J. Garcia, A. Cummings, J. Barrios-Vargas, M. Panhans, A. Harju, F. Ortmann, S. Roche, *Physics Reports* 903 (2021) 1–69, <https://doi.org/10.1016/j.physrep.2020.12.001>.
- [55] A. Lherbier, S.M.-M. Dubois, X. Declerck, S. Roche, Y.-M. Niquet, J.-C. Charlier, *Phys. Rev. Lett.* 106 (2011), 046803.
- [56] D. Van Tuan, A. Kumar, S. Roche, F. Ortmann, M.F. Thorpe, P. Ordejon, *Phys. Rev. B* 86 (2012) 121408.
- [57] J. Kotakoski, A.V. Krasheninnikov, U. Kaiser, J.C. Meyer, *Phys. Rev. Lett.* 106 (2011) 105505.
- [58] A. Antidormi, L. Colombo, S. Roche, *2D Materials*, 2020.
- [59] A. Lherbier, S. Roche, O.A. Restrepo, Y.-M. Niquet, A. Delcorte, J.-C. Charlier, *Nano Research* 6 (2013) 326.
- [60] E. Holmström, J. Fransson, O. Eriksson, R. Lizárraga, B. Sanyal, S. Bhandary, M.I. Katsnelson, *Phys. Rev. B* 84 (2011) 205414.
- [61] F.R. Eder, J. Kotakoski, U. Kaiser, J.C. Meyer, *Sci. Rep.* 4 (2014) 4060.
- [62] S.V. Morozov, K.S. Novoselov, M.I. Katsnelson, F. Schedin, D.C. Elias, J.A. Jaszczak, A.K. Geim, *Phys. Rev. Lett.* 100 (2008), 016602.
- [63] M.T. Lusk, L.D. Carr, *Phys. Rev. Lett.* 100 (2008) 175503.
- [64] P.B. Allen, J.L. Feldman, J. Fabian, F. Wooten, *Philos. Mag. A B* 79 (1999) 1715.
- [65] W. Lv, A. Henry, *New J. Phys.* 18 (2016), 013028.
- [66] L. Sponza, H. Amara, C. Attacalite, S. Latil, T. Galvani, F. Paleari, L. Wirtz, F.m. c. Ducastelle, *Phys. Rev. B* 98 (2018) 125206.
- [67] S. Plimpton, *J. Comput. Phys.* 117 (1995) 1.